ACS APPLIED MATERIALS & INTERFACES

RESEARCH ARTICLE

www.acsami.org

Micro and Nano-Texturization of Intermetallic Oxide Alloys by a Single Anodization Step: Preparation of Artificial Self-Cleaning Surfaces

Adriano F. Feil,[*,†] Daniel E. Weibel,[*,§] Rodrigo R. Corsetti,[†] Matheus D. Pierozan,[†] Alexandre F. Michels,[‡,⊥] Flavio Horowitz,[‡] Lívio Amaral,[†] and Sérgio R. Teixeira[*,†]

[†]Laboratório de Filmes Finos e Fabricação de Nanoestruturas (L3Fnano), UFRGS, Instituto de Física, Av. Bento Gonçalves 9500, P.O. Box 15051, 91501-970, Porto Alegre, RS, Brazil

[‡]Laser Spectroscopy and Film Optics Laboratory, UFRGS, Instituto de Física, Av. Bento Gonçalves 9500, P.O. Box 15051, 91501-970, Porto Alegre, RS, Brazil

[§]Laboratório de Fotoquímica e Superfícies (LAFOS), UFRGS, Instituto de Química, Universidade Federal do Rio Grande do Sul, UFRGS, Avenida Bento Gonçalves 9500, P.O. Box 15003, 91501-970, Porto Alegre, RS, Brazil

[⊥]Departamento de Engenharia Química - Centro de Ciências Exatas e Tecnologia, Universidade de, Universidade de Caxias do Sul, UCS, Caxias do Sul, RS, Brazil

Supporting Information

ABSTRACT: Micro- and nanostructures of Ti-γCu (γ = 0, 30, 50, 70, and 100 wt %) intermetallic alloys were produced through a single anodization step. It was found that the original alloy composition influences the final oxide morphology obtained after anodization which presented formation of a microstructure with nanotubes, nanoparticles or nanopillars on the surface. Pure Ti and Cu oxide metals and their alloys presented hydrophilic or superhydrophilic properties immediately after anodization. When the anodized pure metal and/or Ti-γCu surfaces were functionalized with trimethoxypropylsilane (TPMSi), by dipping and coating with a thin perfluorinated layer, the treated substrates became in all cases superhydrophobic (water contact angles in the range of 152−166°), showing excellent self-cleaning properties with hysteresis below 3°. These results can be explained by a combination of nanomicro morphologies with low surface energy compounds in the topmost monolayers. The decrease in hysteresis was associated with a higher M−OH bond concentration on the anodized surfaces, which allowed for more complete TMPSi coating coverage. This study also indicates that easy and effective fabrication of superhydrophobic surfaces in pure metals and alloys is possible without involving traditional multistep processes.

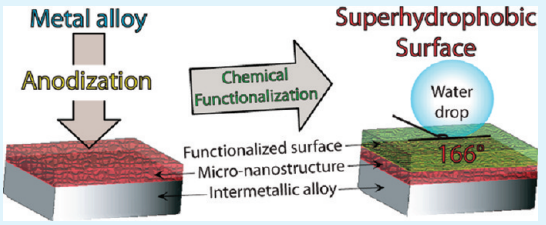

INTRODUCTION

The development of techniques for processing materials has progressed through many significant advances in recent years. Since the 1990s, microfabrication processes have been established with regard to optimization of systems, mainly in microelectronics.[1−3] Today, a trend shift can be identified toward the development of processes that enable the manufacture of devices that combine micro- and nanostructures in the same device. Current techniques for processing structured surface materials are mainly based on electrospray,[4,5] ion beam,[6−8] lithography,[1,9,10] atomic force microscopy (AFM)[11] or by directly reducing the probe-specimen interaction area, as, in scanning tunneling microscopy (STM).[12,13] The use of light, as compared to matter-particle beams or tips,[14−16] can be extremely accurate. These methods are normally expensive and not industrially applicable for devices with large areas. Another limitation of these processes is that they do not favor manufacture, in a single step, of micro- and nanostructured devices.

On the other hand, the anodization process enables the fabrication of nanostructured surface materials over large areas and at relatively low operating costs. Numerous studies have revealed the basis for fabrication of alumina nanopores and nanotubes from the anodization of aluminum (Al).[17−24] Because of the need for materials with specific characteristics, several studies have been reported using anodization of different metals[25−31] and intermetallic alloys.[32−35] In particular, recent interest in the preparation of surfaces with "water repelling" properties has emerged. Advances in techniques and processes to control surface morphology have allowed the fabrication of structures with high hydrophobicity. In this application, the presence of micro- and nanostructure combined with a top layer of a low surface free energy compound is crucial.[36] Inspired by superhydrophobic living organisms in nature, such as lotus leaves[37,38] and water-strider legs,[39] artificial surfaces with superhydrophobic (water contact angle, WCA, > 150° and low angular hysteresis) and superoleophobic[40,41] properties are commonly fabricated via two kinds of approaches: preparation of micro- and

Published: September 15, 2011

nanostructures[42−44] on hydrophobic substrates, or chemical modification of a micro- and nanostructured surface with materials of low surface free energy.[4,37,45,46] Superhydrophilic and superoleophilic surfaces have also been fabricated via increasing both surface roughness and surface free energy. The mechanism here is commonly referred to as a 2D[47] or 3D[48] capillary effect.

In this study, we aimed to fabricate a micro and nanostructures from Ti-γCu intermetallic alloys through a single anodization process, and to investigate the influence of alloy composition on final surface morphology, as well as its chemical functionalization with regard to superhydrophobicity. It was found that the composition of the alloy directly influences the final morphology and structure obtained. Varying the alloy composition and using only a single synthesis process, the formation of microstructures with nanotubes, nanoparticles or nanopillars were observed on the surfaces. By chemical functionalization of the resultant micro- and nanostructures, the surfaces acquired superhydrophobic (WCA = 166° ± 2°) and self-cleaning properties.

EXPERIMENTAL SECTION

Ti-γCu Intermetallic Alloy Preparation. Ti-γCu intermetallic alloys were prepared from pure Ti (99.6%) and Cu (99.5%) powders by an arc-melting apparatus equipped with a vacuum system. The intermetallic compounds were prepared with different Ti and Cu percentages: Ti-γCu alloys (γ = 0, 30, 50, 70, 100 wt %). First, the samples were ground with a series of SiC sandpapers and then polished with diamond paste of 9, 3, and 0.25 μm to obtain mirrorlike finish surfaces. Finally, all samples were ultrasonicated in acetone, rinsed in deionized water (DI), and dried in a N_2 stream.

Micro- and Nanostructure Formation. Micro and nanostructures were obtained by the anodization process using an electrochemical cell that consisted of a conventional two-electrode configuration with platinum gauze as the counter electrode and a metallic substrate as the work electrode. Anodization was carried out at 20 V for 2 h in an electrolyte composed of a mixture of ethylene glycol (ETG) + 10 wt % H_2O + 0.25 wt % NH_4F. All the experiments were carried out at room temperature. After anodization, the samples were rinsed and dried in N_2 stream.

Chemical Functionalization. Anodized substrates were functionalized in a first step with trimethoxypropylsilane (TMPSi) obtained from Aldrich (97%). Silanes are normally stored in the nonhydrolyzed state, and in most cases need to be hydrolyzed in dilute aqueous solutions before application.[49] Diluted TMPSi aqueous solutions were prepared by adding the silane to a mixture of ethanol and DI water. The solution was magnetically stirred for a few minutes and then aged in dark conditions to ensure formation of a sufficient number of active Si−OH groups. Complete hydrolysis was not necessary with the benefit that a solid rather than an oily silane film was formed on metal substrates.[49] The treated and cleaned substrates were subsequently coated with TMPSi using a custom-built dip coating machine, rinsed extensively with DI water and finally baked in air atmosphere to increase the condensation reaction rates. As a final step of the functionalization process, the treated substrates were covered by a thin layer of polytetrafluoroethylene (PTFE) using the Physical Vapor Deposition (PVD) method. PTFE was evaporated from a molybdenum boat by thermal evaporation at a base working pressure of about 0.4×10^{-5} Pa. During deposition, the substrate was held perpendicular and stationary above the source.

Characterization. Morphological characterization of the anodized samples (pure and alloys) was carried out by Scanning Electron Microscopy (SEM, JEOL JSM 6060). An energy-dispersive spectroscopy (EDS) analyzer fitted to the SEM chamber was used for composition analysis of samples. SEM and EDS techniques were operating at 20 kV acceleration voltages. The crystalline structure of the Ti-γCu alloys was determined by X-ray diffraction (XRD) analysis in a Philips X'pert MRD diffractometer operating at 50 kV and 20 mA with Cu Kα radiation (λ = 1.54178 Å) in the range of $30° \leq 2\theta \leq 80°$. X-ray photoelectron spectroscopy (XPS) was performed in a conventional electron spectrometer (Omicron) equipped with a high-performance hemispherical energy analyzer with a seven-channeltron detector and using Mg Kα radiation as the excitation source. Survey spectra were recorded with pass energy of 50 eV, whereas selected atomic signals were acquired with 10 eV of pass energy. In the spectra, the position of the C−C/C−H was specified, and other peaks were fixed relative to this peak, set at 285.0 eV. The C 1s envelope was analyzed and peak-fitted after subtraction of a Shirley background using Gaussian−Lorenzian peak shapes obtained from the CasaXPS software package.

Water contact angles (WCA) were measured using the sessile drop method by deposition of 4−6 μL droplets of DI water on a horizontal surface, and under their observation in cross-section. Each drop was observed directly with an Olympus BX-41 microscope objective lens, whereas its image was digitally captured using a 1.4 mega pixel computer-controlled digital CCD camera. The values reported are averages of more than twenty measurements performed in different areas of each sample surface. The sliding angle measurements were performed using a mechanical level goniometer. Advancing and receding contact angles were measured on both sides of the drop and on at least three different locations for each sample.

Cu(II) complex concentration in water solutions was measured by a UV-1601PC-VIS spectrophotometer (Shimadzu Co. Japan).

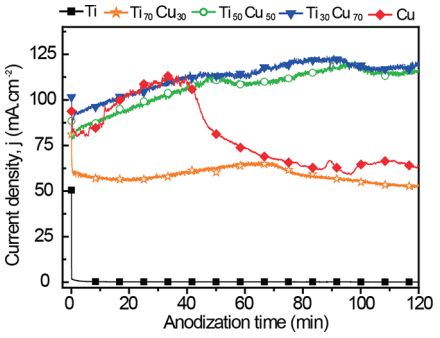

Figure 1. Current density−time curves of pure metals and Ti-γCu alloys recorded at 20 V for 120 min. Solution composition: ETG + 10 wt % H_2O + 0.25 wt % NH_4F.

RESULTS AND DISCUSSION

Anodization of Ti-γCu Alloys. Figure 1 shows typical current−time curves of Ti-γCu alloy anodization, recorded at 20 V for 120 min. The sample of pure Ti shows current density stabilization at 1.5 mA cm^{-2}, whereas increasing concentration of Cu implies an upward fluctuation in current density. This fluctuation probably occurs because of the increase in solubility of the alloy, which is greater than that of the Ti metal, in the anodization solution. The significant increase in current density can cause breakdown[20,23] of the anodized layer or formation of microscopic defects due to localized heating. Rupture of the anodized films was not observed under the experimental conditions studied here. Pure Cu samples showed significant variations in current density at the beginning of anodization. However, after about 40 min of anodization, the current density decreased, showing a different behavior when compared with pure Ti and

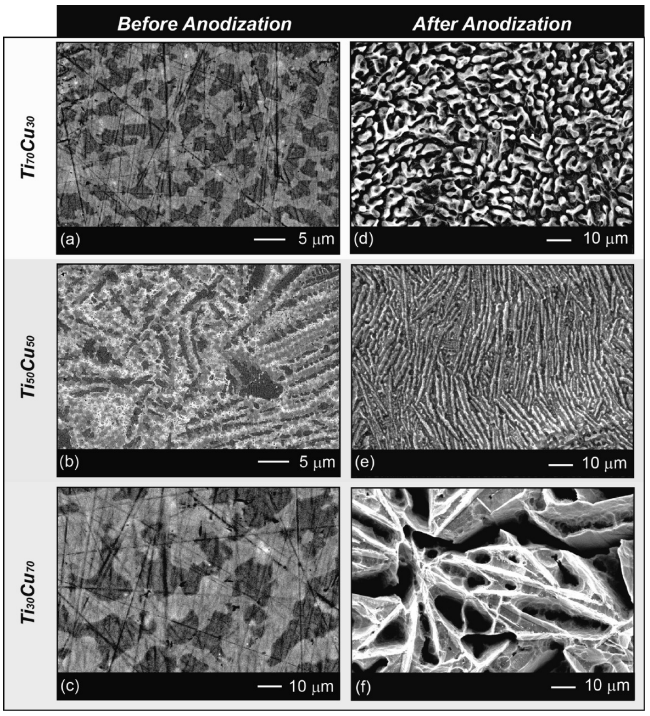

Figure 2. Large-scale SEM backscattering images of the surface samples before anodization: (a) $Ti_{70}Cu_{30}$, (b) $Ti_{50}Cu_{50}$, and (c) $Ti_{30}Cu_{70}$; and after anodization: (d) $Ti_{70}Cu_{30}$, (e) $Ti_{50}Cu_{50}$, and (f) $Ti_{30}Cu_{70}$.

Table 1. Results of EDS Composition of Intermetallic Alloys Analyzing the Light and Dark Regions and the Average Total Composition of the Alloys

	alloy composition (wt %)		
sample	dark gray	bright gray	total
$Ti_{30}Cu_{70}$	$Ti_{34}Cu_{66}$	$Ti_{13}Cu_{87}$	$Ti_{30}Cu_{70}$
$Ti_{50}Cu_{50}$	$Ti_{59}Cu_{41}$	$Ti_{37}Cu_{63}$	$Ti_{50}Cu_{50}$
$Ti_{70}Cu_{30}$	$Ti_{84}Cu_{16}$	$Ti_{56}Cu_{42}$	$Ti_{70}Cu_{30}$

Ti-γCu alloys. The formation of a homogeneous layer of copper oxide on the surface of the pure Cu sample may explain these results.

Microstructure Formation. Figure 2a−c shows surface SEM backscattering images of samples $Ti_{70}Cu_{30}$, $Ti_{50}Cu_{50}$, and $Ti_{30}Cu_{70}$ before the anodization process. The EDS (see Table 1) showed that the two different regions with microscopic dimensions appearing on the sample of the sample surface were, respectively, a Cu-rich phase (bright gray) and Ti-rich phase (Dark Gray). XRD analysis showed that the alloys exhibit a heterogeneous crystalline structure composed of more than one phase (see details in the Suporting information, Figure S1), corroborating data from EDS.

After anodization, a drastic change in morphology was observed (Figures 2 d-f). The shape and size of the microstructures approximately coincided with the dimensions of the bright regions (Cu rich phases) of Figure 2a−c. These microstructures can be ascribed to considerable Cu dissolution during anodization in agreement with the current−time curves presented in Figure 1. Changes produced in the anodized substrates depended on alloy composition. In Figure 2d, formation of a microstructure with irregular variations on the micrometer scale can be seen. In Figure 2e, more regular channel-like structures (lamellae) were observed. The lamellar structures observed in Figure 2b were formed from a competitive growth mechanism, during diffusion, where the Cu atoms rejected during the formation of α-Ti are incorporated into the Ti_2Cu structure through a diffusive flux.[50] The microstructure observed in Figure 2e is the result of anodization of the sample, where Cu dissolution is also observed, in agreement with Figure 1. Finally, Figure 2f shows surface defects with holes larger than 10 μm. These micrometer structures were observed only in Ti-γCu alloys, and were mainly due to the dissolution of Cu into the anodizing solution as explained below. Ti dissolution also occurs and is a well-known effect during the anodization process, but it is low compared with Cu dissolution, as can be seen in the current−time transient curves in Figure 1.

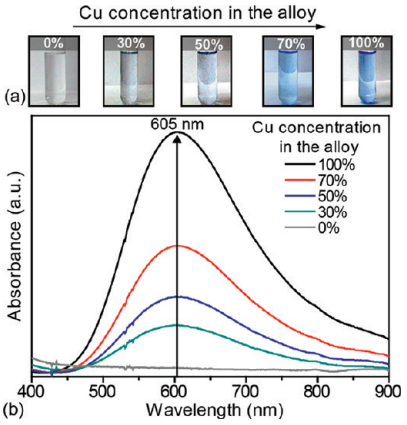

Figure 3. (a) Photographs of the anodization solution with addition of NH3 after performing the anodization process, and (b) UV−vis spectra of anodized solutions identifying the absorption peak at 605 nm due to formation of $Cu(NH_3)_4^{3+}{}_{(aq)}$ complexes.

Figure 3a shows a sequence of photographs of anodizing solutions when concentrated NH_3 solutions were added after anodization. It was observed that, with increasing Cu concentration in the alloy, the solution became more bluish. This effect was related to $Cu(NH_3)_{4(aq)}^{2+}$ complex formation that has maximum absorption at 605 nm (Figure 3b).[51] The Cu complex concentration increased from zero to 1.9×10^{-3} mol L^{-1} when the Cu concentration in the alloy changed from 0 to 100%.

The microstructure formed after anodization could be explained by the high dissolution of Cu located in sections of the Cu-rich alloy during anodization, which may increase the current density (Figure 1) of the Ti-γCu alloys and pure Cu. The sizes of the defects were directly related to the Cu-rich fields, as shown in the backscattering SEM images of Figure 2a−c.

Nanostructure Formation. A zoom image of the anodized samples in Figure 2d−f can be seen in Figure 4. The formation of structures on the nanometer scale with different morphological characteristics could be observed. Presence of different Cu amounts in Ti-γCu intermetallic alloys strongly affects final nanostructure formation. Figure 4a shows that in the $Ti_{70}Cu_{30}$ sample, formation of nanotubes (NTs) occurs mainly in the regions of low copper concentration as shown in Figure 2a. The

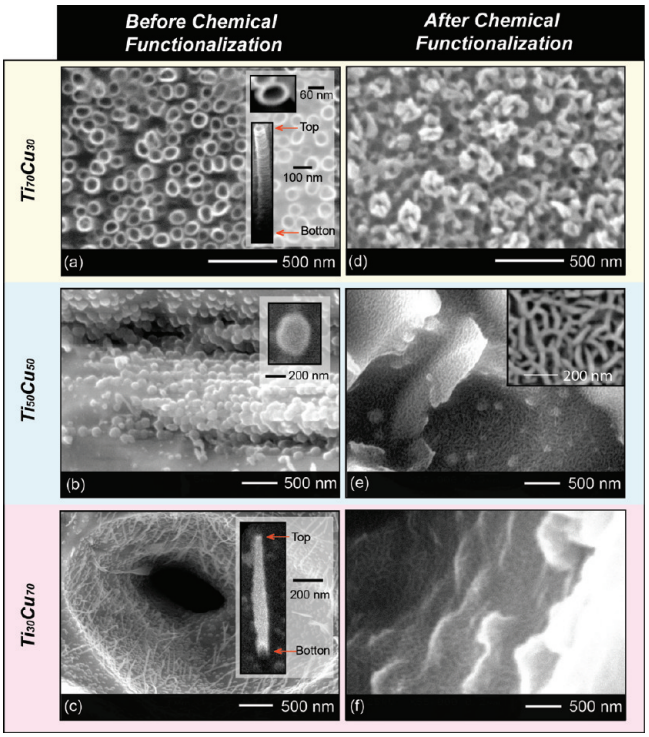

Figure 4. SEM images of anodized alloys (a) $Ti_{70}Cu_{30}$, (b) $Ti_{50}Cu_{50}$, and (c) $Ti_{30}Cu_{70}$. On the right side of each figure, details of the formed nanostructures can be seen. (d−f) SEM images corresponding to the functionalized alloys a−-c.

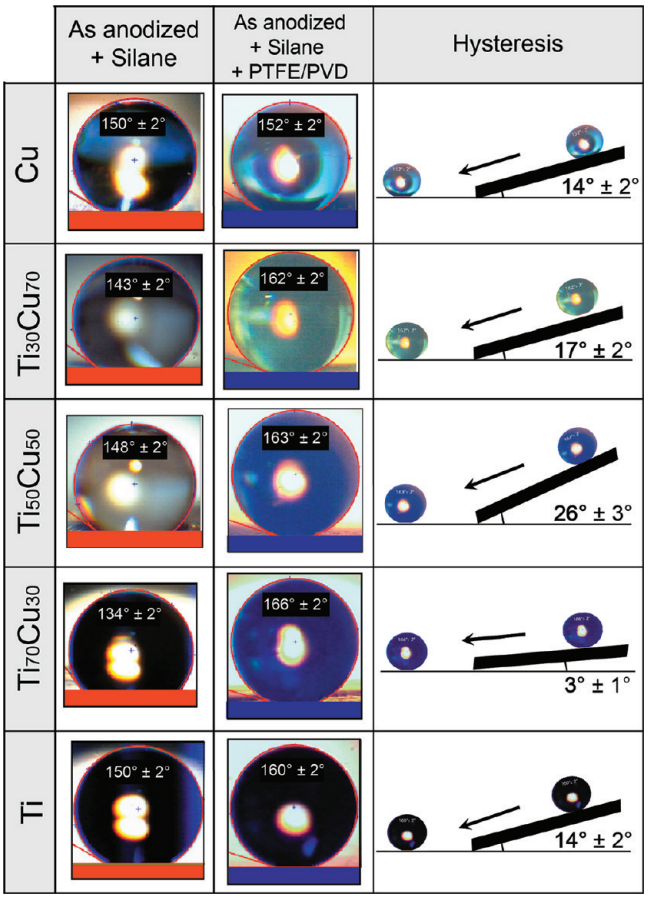

Figure 5. Schematic overview of the images of water droplets on the sample surfaces with different treatments, depending on composition of the anodized sample. The hysteresis of the anodized substrates, functionalized with TMPSi dipping and PTFE/PVD, are shown in the last column.

NTs present a length of 1 μm, a diameter of 60 nm, and a wall thickness of 10−15 nm, as can be seen in detail on the right side of Figure 4a. The structure is similar to NTs formed from pure Ti under the same anodization conditions.[33] When the $Ti_{50}Cu_{50}$ alloy was anodized, the final morphology consisted of small particles with a diameter of about 200 nm (see detail in Figure 4b) dispersed along the surface of the microchannels. Finally, when 70% of Cu was present in the alloy, the formation of structures such as nanofibers located in the walls of large holes were found, as can be seen in Figure 2f. The nanofibers had a diameter of 20 nm and a total length of 1.5 μm. Additionally, Figure 4d−f shows the surface of alloys after the chemical functionalization process. In all images, a snakelike structure could be observed superimposed on the original anodized alloy substrates (see details in the inset of Figure 4e). The same results were also found in our previous study of Al substrates.[36]

Superhydrophobic Surface. The anodization process of the Ti-γCu alloys led to a complex and diverse combination of micro/nano structures. Those novel synthesized structures open a number of scientific and technological applications in the field of nanotechnology. One very interesting example with practical application, that combines micro- and nanostructured morphology, is the study of superhydrophobic surfaces.

Trying to test the wetting properties of the prepared alloys, a series of experiments was carried out. Two sets of samples were prepared: (i) as anodized, and (ii) chemically functionalized with TMPSi and PTFE (PVD method). When the WCAs of the anodized samples were measured immediately after anodization, the surface of all samples showed hydrophilic or superhydrophilic properties. After aging in air, the wetting properties of the samples slowly changed to hydrophobic with WCAs in the range of 110−140°, depending on the environmental conditions and aging time. This hydrophobicity may be caused by hydrocarbon contamination from the atmosphere and is not generally useful because there is not a covalent bond between the surface and the organic layer. Instead, a permanent link between the anodized surface and the organic lower surface layer can be obtained by process ii. Figure 5 shows static WCA data of samples anodized and then chemically functionalized with TMPSi and the PTFE/PVD method. When anodized Ti and Cu samples were chemically functionalized with TMPSi, there was a significant increase in both WCAs to 150 ± 2°. The alloys also showed hydrophobic properties, almost reaching superhydrophobicity in the case of $Ti_{50}Cu_{50}$. This effect was associated with a reduction in surface energy due to the formation of a silane layer that had already been observed in anodized Al substrates.[36] Finally, the samples treated with silane were functionalized with PTFE/PVD, and thus the WCAs increased even more, reaching superhydrophobic properties in all treated substrates. Figure 5 shows that all samples containing Ti and functionalized with silane plus PTFE/PVD had WCAs exceeding 160°.

Another interesting and important feature of a superhydrophobic surface is the self-cleaning property commonly found in

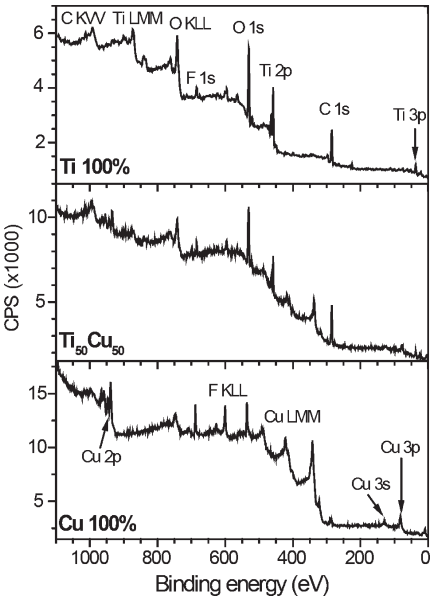

Figure 6. XPS wide scan spectra of Ti (top), $Ti_{50}Cu_{50}$, (middle), and Cu (bottom) anodized substrates before chemical functionalization. Characteristic signals of each element are indicated in the figure.

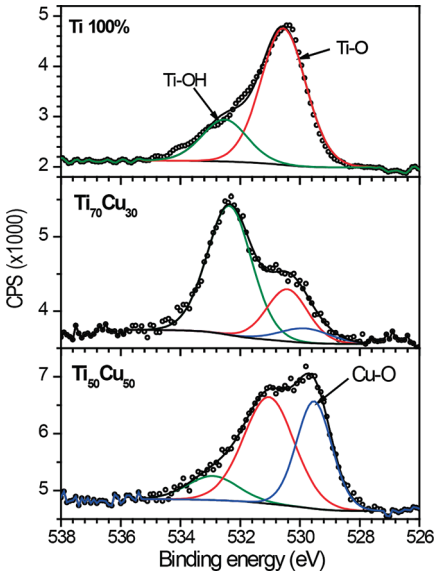

Figure 7. XPS spectra of the O 1s signal from anodized surfaces of pure Ti and its alloys before chemical functionalization.

nature. One simple way to measure hysteresis is by tilting the sample and measuring when the water drop is about to start moving down. Figure 5 shows hysteresis of the pure metal and of the alloys functionalized with TMPSi and PTFE/PVD method. On a self-cleaning surface, a water drop moves easily over the surface at angles less than 10°. $Ti_{70}Cu_{30}$ anodized alloys that were chemically functionalized showed sliding angles of about 3°, presenting excellent self-cleaning properties, since the water drop could move easily over the surface, dragging dirt particles. Pure metals and other alloys showed higher hysteresis (see Figure 5). Silane only treated samples showed even higher hystersis.

To gain insight into the origin of the different hysteresis values found in the functionalized samples, XPS analyses were carried out before functionalization. After functionalization with TMPSi and the PTFE/PVD method, the treated surfaces showed typical XPS spectra of perfluorinated layers, similar to those previously found in Al functionalized substrates.[36] Figure 6 shows a typical XPS wide scan spectra of pure Ti, pure Cu, and $Ti_{50}Cu_{50}$ alloy before chemical functionalization. As can be seen in Figure 6, the surfaces of the anodized samples were contaminated with residues of the anodizing medium or hydrocarbon adsorption after anodization (mainly F and/or C). The XPS spectra also show that, in the alloys, the surfaces of the anodized samples had contributions of both metals in a concentration that depended on the original alloy concentration. To understand the low hysteresis obtained for the $Ti_{70}Cu_{30}$ alloy, XPS core signals before functionalization were analyzed in more detail. Particularly, the O 1s signal was very illustrative. Figure 7 shows the XPS spectra of the O 1s signal of anodized pure Ti substrate and two alloys before the functionalization treatment with TMPSi and PTFE/PVD. As can be seen in Figure 7 (top), the O 1s signal can be satisfactorily fitted with two peaks that can be assigned to Ti−O and Ti−OH bonding.[52] That spectrum (Figure 7, top) corresponds to a typical TiO_2 XPS spectrum. When Cu is present in the alloy, a new signal at about 529.6 eV can be assigned to Cu−O bonding.[53] Anodized pure Cu showed mainly one contribution in the deconvoluted O 1s signal (Cu−O, 94%) and a small component shifted to higher energy (Cu−OH, 6%) that could be attributed to hydroxide and/or chemisorbed oxygen.[53] Anodized pure Cu and its alloys mainly present the characteristic XPS spectra of CuO. The Cu $2p_{3/2}$ peaks exhibits a main peak at 933.7 eV accompanied by a satellite on the high binding energy side at about 9 eV (Figure 6). The spectrum of Cu_2O has only one peak located at about (932.4 ± 0.2) eV.[53] The oxygen elemental composition on the surface of the as anodized substrates was determined from the XPS O1s spectra and summarized in Table 2. As can be seen for pure Ti and alloys in Table 2, there was a close correlation between the Ti−OH relative concentration and hysteresis.

It is known that the TMPSi and PTFE/PVD method lead to a thin perfluorinated layer on the topmost monolayers of the treated substrates. Between this perfluorinated layer and the metal substrate exists a silane layer linked to the anodized substrate.[36] The first step in the functionalization process is the dipping of the anodized substrates in diluted silane solutions. It is generally assumed that, upon drying the silane-treated metals, two key condensation reactions occur.[49] One is the formation of covalent metallo-siloxane bonds (M−O−Si) between silanols (Si−OH) from the silane solution and the metal hydroxyls (M−OH) from the metal surface hydroxides. The other is condensation among the excess Si−OH groups adsorbed on the metals, forming a siloxane (Si−O−Si) film on top. As a consequence, the amount of M−O−Si bonds formed depends on the M−OH concentration on the surface and they may determine the performance of the coating. Our hypothesis, based on the XPS O 1s results, is that the lowest hysteresis obtained (see Table 2) is due to a more complete coating with TMPSi of the anodized $Ti_{70}Cu_{30}$ alloy surface that has the highest M−OH contributions. When the M−OH concentration decreased, the coating coverage was less complete and, although the surfaces presented superhydrophobicity, there could be regions in which the water drop was interacting with a less hydrophobic surface, and therefore hysteresis increased.

Table 2. XPS Peak-Fitted Components of the O 1s Spectra for Anodized Substrates before Chemical Functionalization

sample	Ti−O	Ti−OH	Cu−OH	Cu−O	ratio Ti−OH/ Ti−O	hysteresis (deg)
Cu_{100}			6	94		14 ± 2
$Ti_{30}Cu_{70}$	41	21	2	36	0.5	17 ± 2
$Ti_{50}Cu_{50}$	52	11	1	36	0.2	26 ± 3
$Ti_{70}Cu_{30}$	29	60	4	7	2	3 ± 1
Ti_{100}	76	24			0.3	14 ± 2

These results highlight the importance of the proper combination of micronano morphology and surface chemical functionalization with low surface free energy compounds. The fully treated alloy surfaces showed static and dynamic superhydrophobic properties. When the roughness factor was increased by the presence of the nanostructure, the decrease in the solid−liquid contact area, and the simultaneous increase of the liquid−air interface, switched from the dominant Wenzel's[54] regime to the so-called Cassie−Baxter's[55] regime. The low hysteresis effect, obtained when the Cassie−Baxter's regime became dominant, was magnified by the presence of a thin layer of a low surface energy chemical compound, a PTFE-like overlayer.

CONCLUSIONS

In summary, we have shown a simple and highly reproducible method for the fabrication of a surface that combines micro and nanostructures from a single anodization step for Ti-γCu intermetallic alloys. In these alloys the formation of microstructures is due to high dissolution of Cu in the Cu-rich phases during the anodizing process. On the other hand, formation of the nanostructure occurs in the Ti-rich phase and in the Ti-γCu alloy. The study of wettability of those structures, after chemical functionalization with TMPSi dipping and PTFE/PVD treatment, showed that functionalized and anodized alloys were superhydrophobic with WCAs always greater than 160°, and low to very low hysteresis (from 26° to less than 3°). This degree of hysteresis, on the anodized surface, was associated with a low concentration of M−OH bonds present on the surface before the chemical functionalization step with silane. An increase of M−OH bonds allowed for better coverage by the TMPSi coating, and by its bonded PTFE-like overlayer as well. The new process, unlike traditional manufacturing of micro- and nanostructures, opens a new way for the formation of structures with superhydrophobic performance and with low production costs.

ASSOCIATED CONTENT

Supporting Information. Crystalline structure information on the Ti-γCu intermetallic alloys after the anodization process (PDF). This material is available free of charge via the Internet at http://pubs.acs.org.

AUTHOR INFORMATION

Corresponding Author

*E-mail: affeil@if.ufrgs.br (A.F.F.); danielw@iq.ufrgs.br (D.E.W.). Tel: +55-51 3308.6508 (A.F.F.); +55-51 3308.6204 (D.E.W.). Fax: +55-51 3308.7286 (A.F.F.); +55-51 3308.7304 (D.E.W.).

ACKNOWLEDGMENT

This paper was supported in part by the CNPq, CAPES, and FAPERGS Brazilian financial agencies. We also thank the Electron Microscopy Center−CME at UFRGS, for allowing usage of its facilities during this investigation.

REFERENCES

(1) Buschvishniac, I. J. *Sens. Actuator A-Phys.* **1992**, *33*, 207–220.
(2) Khoperia, T. N.; Tabatadze, T. J.; Zedgenidze, T. I. *Electrochim. Acta* **1997**, *42*, 3049–3055.
(3) Xia, Y. N.; Whitesides, G. M. *Annu. Rev. Mater. Sci.* **1998**, *28*, 153–184.
(4) Burkarter, E.; Saul, C. K.; Thomazi, F.; Cruz, N. C.; Zanata, S. M.; Roman, L. S.; Schreiner, W. H. *J. Phys. D: Appl. Phys.* **2007**, *40*, 7778–7781.
(5) Burkarter, E.; Saul, C. K.; Thomazi, F.; Cruz, N. C.; Roman, L. S.; Schreiner, W. H. *Surf. Coat. Technol.* **2007**, *202*, 194–198.
(6) Guillorn, M. A.; Simpson, M. L.; Bordonaro, G. J.; Merkulov, V. I.; Baylor, L. R.; Lowndes, D. H. *J. Vac. Sci. Technol., B* **2001**, *19*, 573–578.
(7) Langford, R. M.; Nellen, P. M.; Gierak, J.; Fu, Y. Q. *MRS Bull.* **2007**, *32*, 417–423.
(8) Dallanora, A.; Marcondes, T. L.; Bermudez, G. G.; Fichtner, P. F. P.; Trautmann, C.; Toulemonde, M.; Papaleo, R. M. *J. Appl. Phys.* **2008**, *104*.
(9) Quake, S. R.; Scherer, A. *Science* **2000**, *290*, 1536–1540.
(10) Senaratne, W.; Andruzzi, L.; Ober, C. K. *Biomacromolecules* **2005**, *6*, 2427–2448.
(11) Chien, F. S. S.; Chang, J. W.; Lin, S. W.; Chou, Y. C.; Chen, T. T.; Gwo, S.; Chao, T. S.; Hsieh, W. F. *Appl. Phys. Lett.* **2000**, *76*, 360–362.
(12) Simeone, F. C.; Albonetti, C.; Cavallini, M. *J. Phys. Chem. C* **2009**, *113*, 18987–18994.
(13) Wiesendanger, R. *Jpn. J. Appl. Phys., Part 1* **1995**, *34*, 3388–3395.
(14) Tanaka, T.; Sun, H. B.; Kawata, S. *Appl. Phys. Lett.* **2002**, *80*, 312–314.
(15) Shimotsuma, Y.; Hirao, K.; Kazansky, P. G.; Qiu, H. R. *Jpn. J. Appl. Phys., Part 1* **2005**, *44*, 4735–4748.
(16) Cardoso, M. R.; Tribuzi, V.; Balogh, D. T.; Misoguti, L.; Mendonca, C. R. *Appl. Surf. Sci.* **2011**, *257*, 3281–3284.
(17) Masuda, H.; Fukuda, K. *Science* **1995**, *268*, 1466–1468.
(18) Thompson, G. E. *Thin Solid Films* **1997**, *297*, 192–201.
(19) Li, A. P.; Muller, F.; Birner, A.; Nielsch, K.; Gosele, U. *J. Appl. Phys.* **1998**, *84*, 6023–6026.
(20) Lee, W.; Ji, R.; Gosele, U.; Nielsch, K. *Nat. Mater.* **2006**, *5*, 741–747.
(21) Li, F. Y.; Zhang, L.; Metzger, R. M. *Chem. Mater.* **1998**, *10*, 2470–2480.
(22) Feil, A. F.; da Costa, M. V.; Amaral, L.; Teixeira, S. R.; Migowski, P.; Dupont, J.; Machado, G.; Peripolli, S. B. *J. Appl. Phys.* **2010**, *107*, 026103.
(23) Feil, A. F.; da Costa, M. V.; Migowski, P.; Dupont, J.; Amaral, L.; Teixeira, S. R. *J. Nanosci. Nanotechnol.* **2011**, *11*, 2330–2335.
(24) Feil, A. F.; Migowski, P.; Dupont, J.; Amaral, L.; Teixeira, S. R. *J. Phys. Chem. C* **2011**, *115*, 7621–7627.
(25) El-Sayed, H. A.; Birss, V. I. *Nano Lett.* **2009**, *9*, 1350–1355.
(26) Wender, H.; Feil, A. F.; Diaz, L. B.; Ribeiro, C. S.; Machado, G. J.; Migowski, P.; Weibel, D. E.; Dupont, J.; Teixeira, S. R. *ACS Appl. Mater. Interfaces* **2011**, *3*, 1359–1365.
(27) Choi, J. S.; Wehrspohn, R. B.; Lee, J.; Gosele, U. *Electrochim. Acta* **2004**, *49*, 2645–2652.
(28) Macak, J. M.; Tsuchiya, H.; Schmuki, P. *Angew. Chem., Int. Ed.* **2005**, *44*, 2100–2102.
(29) Tsuchiya, H.; Schmuki, P. *Electrochem. Commun.* **2005**, *7*, 49–52.
(30) Sieber, I.; Hildebrand, H.; Friedrich, A.; Schmuki, P. *Electrochem. Commun.* **2005**, *7*, 97–100.
(31) Tsuchiya, H.; Macak, J. M.; Sieber, I.; Taveira, L.; Ghicov, A.; Sirotna, K.; Schmuki, P. *Electrochem. Commun.* **2005**, *7*, 295–298.

(32) Berger, S.; Tsuchiya, H.; Schmuki, P. *Chem. Mater.* **2008**, *20*, 3245–3247.
(33) Feil, A. F.; Migowski, P.; Scheffer, F. R.; Pierozan, M. D.; Corsetti, R. R.; Rodrigues, M.; Pezzi, R. P.; Machado, G.; Amaral, L.; Teixeira, S. R.; Weibel, D. E.; Dupont, J. *J. Braz. Chem. Soc.* **2010**, *21*, 1359–1365.
(34) Mor, G. K.; Varghese, O. K.; Wilke, R. H. T.; Sharma, S.; Shankar, K.; Latempa, T. J.; Choi, K. S.; Grimes, C. A. *Nano Lett.* **2008**, *8*, 1906–1911.
(35) Macak, J. M.; Tsuchiya, H.; Taveira, L.; Ghicov, A.; Schmuki, P. *J. Biomed. Mater. Res. Part A* **2005**, *75A*, 928–933.
(36) Weibel, D. E.; Michels, A. F.; Feil, A. F.; Amaral, L.; Teixeira, S. R.; Horowitz, F. *J. Phys. Chem. C* **2010**, *114*, 13219–13225.
(37) Feng, L.; Li, S. H.; Li, Y. S.; Li, H. J.; Zhang, L. J.; Zhai, J.; Song, Y. L.; Liu, B. Q.; Jiang, L.; Zhu, D. B. *Adv. Mater.* **2002**, *14*, 1857–1860.
(38) Marmur, A. *Langmuir* **2004**, *20*, 3517–3519.
(39) Hu, D. L.; Chan, B.; Bush, J. W. M. *Nature* **2003**, *424*, 663–666.
(40) Feng, X. J.; Jiang, L. *Adv. Mater.* **2006**, *18*, 3063–3078.
(41) Ramos, S. M. M.; Benyagoub, A.; Canut, B.; Jamois, C. *Langmuir* **2010**, *26*, 5141–5146.
(42) Ramos, S. M. M.; Charlaix, E.; Benyagoub, A.; Toulemonde, M. *Phys. Rev. E* **2003**, *67*.
(43) Ramos, S. M. M.; Charlaix, E.; Benyagoub, A. *Surf. Sci.* **2003**, *540*, 355–362.
(44) Ramos, S. M. M.; Canut, B.; Benyagoub, A. *J. Appl. Phys.* **2009**, *106*.
(45) Bauer, S.; Park, J.; von der Mark, K.; Schmuki, P. *Acta Biomater.* **2008**, *4*, 1576–1582.
(46) Lee, W.; Jin, M. K.; Yoo, W. C.; Lee, J. K. *Langmuir* **2004**, *20*, 7665–7669.
(47) Wang, R.; Hashimoto, K.; Fujishima, A.; Chikuni, M.; Kojima, E.; Kitamura, A.; Shimohigoshi, M.; Watanabe, T. *Adv. Mater.* **1998**, *10*, 135–+.
(48) Bico, J.; Tordeux, C.; Quere, D. *Europhys. Lett.* **2001**, *55*, 214–220.
(49) van Ooij, W. J.; Zhu, D.; Palanivel, V.; Lamar, J. A.; Stacy, M. *Silicon Chem.* **2006**, *3*, 11–30.
(50) Osorio, W. R.; Cremasco, A.; Andrade, P. N.; Garcia, A.; Caram, R. *Electrochim. Acta* **2010**, *55*, 759–770.
(51) Baker, A. T. *J. Chem. Educ.* **1998**, *75*, 98–99.
(52) Erdem, B.; Hunsicker, R. A.; Simmons, G. W.; Sudol, E. D.; Dimonie, V. L.; El-Aasser, M. S. *Langmuir* **2001**, *17*, 2664–2669.
(53) Ghijsen, J.; Tjeng, L. H.; van Elp, J.; Eskes, H.; Westerink, J.; Sawatzky, G. A.; Czyzyk, M. T. *Phys. Rev. B* **1988**, *38*, 11322.
(54) Wenzel, R. N. *Ind. Eng. Chem.* **1936**, *28*, 988–994.
(55) Cassie, A. B. D.; Baxter, S. *Trans. Faraday. Soc.* **1944**, *40*, 546–551.